Simplified bubbling calculations

Edgard Bonilla

February 2021

1 Introduction

This manuscript presents analytical calculations to estimate the Newtonian noise generated by density fluctuations in a flowing liquid coolant in the vicinity of the test mass of a gravitational-wave interferometer. Such fluctuations would occur during the boiling of the liquid nitrogen in the cryogenic shields suggested in [1], that would serve to hold the test mass at its operating temperature.

These calculations draw insight from the theory of boiling and nucleation[1], as well as theory on the spectrum of general point processes, especially renewal shot noise[2].

In order to keep the discussion clear, we will start the estimates by making a preliminary set of assumptions that we will refine as we gain more insight about the details of the physical processes involved. The hope is that with each estimate the reader will gain more intuition about the parameters that drive this source of Newtonian noise and, ultimately, a picture of the design choices that could be made to suppress this noise coupling in third-generation gravitational-wave interferometers.

The note is structured as follows:

- The second section lays out the simplifying assumptions of the model. These result in the noise being an integral of a regular (Poisson) shot noise process, with an amplitude controlled by the rate of bubble nucleation in the cryogenic array and the characteristic size of the nucleated vapor bubbles.

- The third section dives into the theory of boiling and nucleation in order to gain insight on the parameters driving the noise amplitude, culminating with a first estimate of the Newtonian noise coupling.

- The fourth section reviews the shortcomings of the original shot noise assumption in the light of the theory of boiling and nucleation. We introduce renewal shot noise to provide a more refined Newtonian noise estimate.

---

[1]See [2] or [3] for a comprehensive high level summary.

[2]See [4] for a great seminal paper in the subject and [5] for a modern overview of the ideas and equations we will utilize.

- The fifth and final section is dedicated to a discussion of the results, with an emphasis on the implications for the design of the cryogenics for third generation gravitational-wave observatories.

2 Density Newtonian noise as a shot noise process

2.1 Simplifying assumptions:

To start out calculations, we assume most of the Newtonian noise is generated by 'relevant' segments of pipe that contain liquid nitrogen in the vicinity of the test mass, as depicted in Figure 1.

We will assume that all bubble nucleation occurs in the relevant sections of the pipe. Gas bubbles are created in the tubes and they push the liquid away rapidly compared to the timescales of interest[3]. As a result, the gravitational acceleration caused by a section of pipe in front of the test mass like the one in Figure 1 fluctuates over time, depending on the size of the bubbles growing and moving inside it.

To further simplify the calculations, we will consider only the mass fluctuations of the tube segments, neglecting the noise contribution from the specific motion of the bubbles[4]. Additionally, we assimilate the mass of the tube segments and that of the test mass to point masses for an order-of-magnitude assessment.

Under these assumptions, the spectral density of the displacement of the test mass will be given by:

$$|\delta \hat{x}(f)| = \frac{C_x}{(2\pi f)^2} \frac{G}{d_0^2} |\delta \hat{M}(f)| \tag{1}$$

where d_0 is the distance between the test mass and the liquid and δM represents the fluctuation in the mass of the relevant pipe section. C_x has been included as a geometric factor related to the exact positioning of the pipe section (or sections) relative to the longitudinal direction of the test mass.

To model the mass fluctuation of the contents of a section of the pipe, we start by assuming that liquid nitrogen evaporation accounts for a fraction $\dot{Q}_{\text{evap}}$ of the heat absorption of the shield. So, the rate of mass evaporation is given by:

$$\frac{dM_g}{dt} = \frac{\dot{Q}_{\text{evap}}}{h_{lg}}, \tag{2}$$

where h_{lg} is the latent heat of vaporization of nitrogen. If we assume, as stated before, that the gas pushes the liquid away from the relevant section of the pipe

---

[3]The liquid phase density fluctuations propagate approximately with the speed of sound in liquid nitrogen, which we assume to be orders of magnitude larger than the speed of the fluid flow.

[4]The contribution of bubble motion can be shown to be smaller than that of the bubble mass fluctuation.
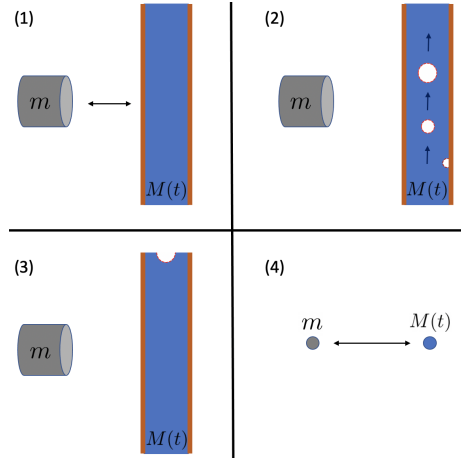
Figure 1: *Schematic of the simplifying assumptions for Newtonian noise calculations. (1) The we will only consider the gravitational interaction of the test mass and a segment (or segments) of pipe near it where all boiling happens. (2) When bubbles grow in the relevant sections, they push away all the incompressible liquid. (3) The mass of the relevant section increases when a bubble leaves it. (4) We will simplify the geometry of the relevant sections and the test mass to that of point particles.*

faster than the timescales we care about; then the volume of gas inside the pipe grows as:

$$\frac{dV_{\text{bub}}}{dt} = \frac{\dot{Q}_{\text{evap}}}{h_{lg}\rho_g} \tag{3}$$

Meaning that the mass that gets pushed out of the pipe due to this growth is given by:

$$\frac{dM_l}{dt} = -\rho_l \frac{\dot{Q}_{\text{evap}}}{h_{lg}\rho_g} \tag{4}$$

Combining these together, we can model the change of mass content in the pipe due to bubble growth and the liquid that gets pushed out.

$$\frac{dM}{dt} = \frac{dM_g}{dt} + \frac{dM_l}{dt} = -\left(\frac{\rho_l}{\rho_g} - 1\right)\frac{\dot{Q}_{\text{evap}}}{h_{lg}} \tag{5}$$

Equation (5) represents the rate of change of the mass of the tube whenever bubbles are not entering or leaving the segment of interest. Bubbles will leave at random times after travelling down the pipe, which ultimately creates an equilibrium void fraction inside the tube. These random leaving times are what will create the fluctuating acceleration that drives the Newtonian noise in this simplified model.

2.2   Shot Noise equations:

We will model the effect of bubbles exiting the relevant section by assuming bubbles inside the pipe have a characteristic size V_0 and leave at random, independently distributed and memoryless times t_i. In this case, we modify equation (5) and obtain the more general equation:

$$\frac{dM}{dt} = -\left(\frac{\rho_l}{\rho_g} - 1\right)\frac{\dot{Q}_{\text{evap}}}{h_{lg}} + (\rho_l - \rho_g)V_0 \sum_i h(t - t_i) \tag{6}$$

3

Where h is a window function that represents the derivative of the mass when a bubble leaves the tube. Naturally, a steady state is found only if the average mass of the tube does not grow with time. Which means as much gas volume is leaving the tube as it is being generated inside. Using the equation for the average of the Poisson process (Campbell's theorem) [6] leaves for the steady state:

$$\dot{Q}_{\text{evap}} = h_{lg}\rho_g V_0 \frac{dN}{dt}. \tag{7}$$

Where $\frac{dN}{dt}$ is the rate of bubble nucleation[5] inside the relevant section, which can be estimated by using the nucleation site density n and the average nucleation rate per site f_{nuc}. To obtain equation (7) we used the fact that $\int h(\tau)d\tau = 1$, since the window function represents a bubble fully leaving the pipe.

Note that (7) is exactly what we would expect for the power absorption by vaporization in the relevant section of the tube. It is simply the energy needed to evaporate bubbles of volume V_0 at a rate given by $\frac{dN}{dt}$.

The (single-sided) amplitude spectral density of the shot noise process (6) with zero mean is given by [6]:

$$\left| \delta\left(\frac{d\hat{M}}{dt} \right)(f) \right| = \sqrt{2}(\rho_l - \rho_g)V_0 \sqrt{\frac{dN}{dt}} |h(f)|. \tag{8}$$

Integrating equation (9) gives the mass fluctuation of a segment of tube:

$$\left| \delta\hat{M}(f) \right| = \frac{1}{2\pi f}\sqrt{2}(\rho_l - \rho_g)V_0 \sqrt{\frac{dN}{dt}} |h(f)|. \tag{9}$$

For simplicity, let us consider the extreme case where the window function $h(t)$ is a delta function (which represents the bubbles leaving the tube instantly[6]). In this case the spectrum (8) is flat and the amplitude spectrum for the test mass displacement is simply:

$$|\delta\hat{x}(f)| = \sqrt{2}\frac{C_x}{(2\pi f)^3}\frac{G}{d_0^2}(\rho_l - \rho_g)V_0 \sqrt{\frac{dN}{dt}} \tag{10}$$

Where, as mentioned before, d_0 is a characteristic distance between the test mass and the cryogen and C_x is a dimensionless $\mathcal{O}(1)$ geometric factor related to the geometric arrangement the liquid tubes relative to the mass.

2.3   Discussion:

The simple shot noise estimate has a couple of features that remain true even among more involved calculations.

---

[5]It is technically the rate at which bubbles leave the relevant pipe section. It will equal the nucleation rate if bubbles don't coalesce or break up as they travel inside the pipe.

[6]This is an extreme case, which represents an upper limit for our noise estimate

First, there is the general $1/f^3$ dependence of the Newtonian noise, which is common for other forms of gravity gradient noise. In reality, we expect even higher suppression for this noise at high frequencies, due to the fact that bubbles do not leave the relevant section of the tube instantly, but rather their influence decays over time as they move away from the test mass.

Additionally, we appreciate that the noise is directly proportional to the characteristic volume[7] V_0 of the bubbles in the relevant section, as well as to the square root of the nucleation rate $\frac{dN}{dt}$. The closure relation for the power absorbed (7) implies that for a given amount of power $\dot{Q}_{\text{evap}}$ the aforementioned variables are not independent. In general, to obtain values for the nucleation rate and the absorbed power it is necessary to specify the details of the geometry of the cryo array.

However, it is possible to get an order of magnitude estimate for V_0 and $\frac{dN}{dt}$ under a generic set of assumptions by examining the details of the boiling process.

3   Boiling and Nucleation:

A large portion of the literature on boiling and nucleation is devoted to the study of the conditions for safe and efficient operation of cooling systems. In consequence, the focus of the theory is often placed on the heat transfer characteristics of the process rather than on the mechanical details of it. This latter ones being the ones we need for the Newtonian noise estimates. Moreover, many results are obtained from fully empirical correlations, and theoretical models only have limited success in reproducing experimental observations.

Therefore, our main objective in this section is to obtain reasonable values for V_0 and $\frac{dN}{dt}$, with the understanding that our estimates are good only within an order of magnitude.

The interested reader is referred to [2] for an in-depth review of the concepts showcased here. Since most of the classical theory of boiling was developed for water and high power applications like nuclear reactors, we will complement it with specific research on cryogenic liquids when necessary.

3.1   Nucleation in flow boiling

Flow boiling corresponds to a situation where a fluid (the coolant) is ran through a device to be cooled, and at some point in the flow, the liquid changes phase. The inception of boiling greatly enhances the heat transfer characteristics of the fluid. The magnitude and mechanisms for this improvement vary depending on the flow regime and even the orientation of the flow.

In what follows, we will only consider the regime where nucleate boiling[8] happens. That is, when boiling happens at the surface of vapor trapped in

---

[7]As per [6], in general it is the RMS value of the volume that enters the spectral density equation.

[8]As opposed to film boiling and forced convection evaporation.

individual holes and crevices of the pipe walls, otherwise known as nucleation sites.
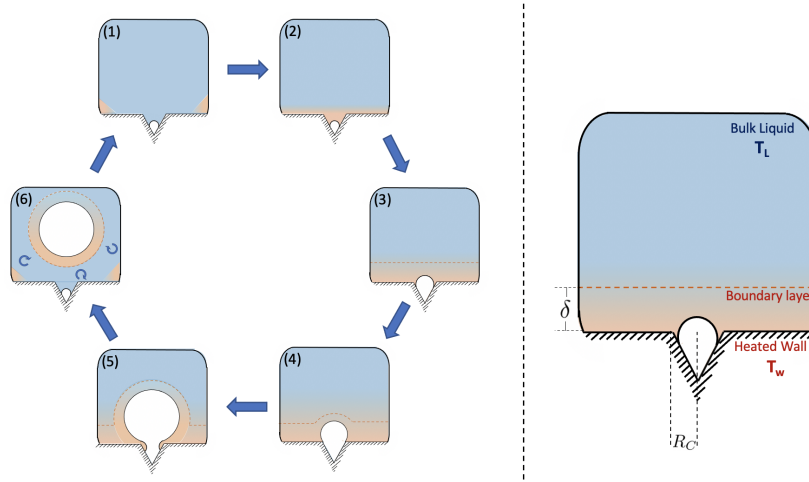

Figure 2: *Simplified depiction of the nucleation cycle. (1) Nucleation starts with vapor trapped in crevices on the heated surface. (2) The heat of the wall starts creating a superheated boundary layer of liquid. (3) The trapped vapor starts growing once the boundary layer is hot enough to support bubble growth against the surface tension. (4) The bubble will continue to grow beyond the size of the cavity, picking up the boundary layer. (5) When the buoyancy of the vapor is enough to overcome the forces attaching the bubble to the surface, the bubble initiates its departure. (6) As the bubble departs from the nucleation site, it disrupts the boundary layer on the wall, cold liquid rushes in on its wake, and the cycle starts anew.*

Figure 2 shows a cartoon of the process of nucleate boiling. It is generally divided in three stages: a waiting period to establish a superheated boundary layer (1 and 2 in the figure), bubble growth (3 and 4) and bubble departure (5 and 6). After the bubble departs it disturbs the superheated layer, cold liquid flows in, triggering another waiting period and restarting the cycle. We will provide an overview of each step of the process, which will ultimately lead to an estimate of V_0 and $\frac{dN}{dt}$

3.2 Nucleation site activation and the waiting period.

When cold liquid flow is in contact with a superheated wall, a thin thermal boundary layer forms [2]. This layer has a temperature gradient that goes from the temperature of the heated surface T_w to that of the bulk liquid T_l which for most purposes can be approximated as being linear. Similarly, the no slip condition at the surface makes it so near the heated walls the liquid can be considered as quiescent.

Since the type of nucleation we will study (heterogeneous nucleation) is an interfacial phenomenon, most of the equations in what follows will depend on the thickness δ of the thermal boundary layer. Its value can be estimated by $\delta = \frac{H_{\text{fc}}}{\kappa_l}$. Where H_{fc} is the forced-convection heat transfer coefficient and κ_l is the thermal conductivity of the liquid.

Nucleation starts when a vapor bubble trapped in a nucleation site is surrounded by superheated liquid hot enough that the vapor pressure inside the bubble can overcome the surface tension of the boundary. The equilibrium condition for the vapor pressure and surface tension is usually expressed with by using the Clausius-Clapeyron equation and yields:

$$T_{\text{B}} - T_{\text{sat}} = \frac{2\sigma T_{\text{sat}}}{R_{\text{B}}\rho_g h_{lg}} \tag{11}$$

Which expresses the minimum bubble superheat needed to grow bubbles of a radius R_{B}. Similarly, the radius of the smallest bubble that will not collapse given a superheat of $\Delta T_{\text{sup}} = T_w - T_{\text{sat}}$ is $R^* = \frac{2\sigma T_{\text{sat}}}{\Delta T_{\text{sup}}\rho_g h_{lg}}$.

Bubbles will continue to grow as long as they are surrounded by liquid hotter than their interior. This implies that nucleation will successfully happen only if the thickness δ of the thermal boundary layer is large enough to support the growth of the bubbles.

In that sense, even though less wall superheat is needed to grow bubbles in larger cavities (as per equation (11)), the thickness of the thermal boundary layer imposes an upper limit on the size of the bubbles that can grow. The result is that for a given wall superheat only cavities with a radius R_C in a range $R_{\text{C,max}} \geq R_C \geq R_{\text{C,min}}$ can be active nucleation sites. The size range can be estimated by:

$$R_{\text{C,max}}, R_{\text{C,min}} = \frac{\delta}{2C_1}\frac{\Delta T_{\text{sup}}}{T_w - T_l}\left[1 \pm \sqrt{1 - \frac{C_1}{C_2}\frac{8(T_w - T_l)T_{\text{sat}}\sigma}{\Delta T_{\text{sup}}^2 \delta \rho_g h_{lg}}}\right] \tag{12}$$

Where C_1 and C_2 are geometric constants[9]. Their assumed values vary across different articles in the literature [7][8][9]. We will follow the example of [8], who use $C_2 = 1$ and derive $C_1 = \frac{3}{2}$ based on the isothermal curves around a hemispherical bubble on a cavity.

We also observe that there are regions of physical parameters for which equation (12) does not have any real solutions. Meaning that for a given wall superheat it is not possible to sustain bubble nucleation. This can happen because the thermal boundary layer is too thin[10], or because the temperature gradient in the layer is too steep[11].

The point where the competing effects balance out and nucleation is first possible is called the Onset of Nucleate Boiling (ONB) point and can be found

---

[9]C_1 is the ratio of the distance between the wall and the point where the liquid has the temperature of the bubble interior T_B and the cavity mouth radius. C_2 is the ratio of bubble radius to cavity mouth radius.

[10]This happens when the fluid flow is very fast, enhancing H_{fc}

[11]Which happens when the bulk liquid is highly subcooled

by setting the radical of equation (12) to zero. In a heated channel, we can expect no nucleation to happen upstream of the ONB point.

Despite the range suggested by equation (12), Bald [10] argues that the maximum active cavity radius in the case of cryogenic liquids is determined by their wetting capabilities. Owing to the fact they have very low contact angles [11], they will tend to flood large cavities and deactivate them entirely, giving a value for $R_{C,\max}$ smaller than predicted by (12). This observation will be relevant later when we discuss the suppression of nucleation.

3.2.1 Waiting time

The waiting time is the time needed to establish a superheated layer next to an active cavity. A simple model for it considers the heat conduction to a semi-infinite medium until the thickness of the boundary layer is able to sustain nucleation [8][12]. In this model, the waiting time is approximately given by:

$$t_w = \frac{1}{\pi \alpha_l} \left(\frac{\frac{3}{2} R_C (T_w - T_l)}{T_w - T_{\text{sat}} \left(1 + \frac{2\sigma}{R_C \rho_g h_{lg}} \right)} \right)^2 \tag{13}$$

Note that equation (13) is just the time it takes for the heat of the wall to diffuse and increase the temperature at $y = \frac{3}{2} R_C$ from the wall to the required T_B for bubble growth. $\alpha_l = \frac{\kappa_l}{\rho_l c_{p,l}}$ is the thermal diffusivity of the liquid.

3.3 Bubble growth:

Bubble growth at a nucleation site follows a three-regime pattern. first growing in an inertia-controlled regime (pressure and surface tension dominant), a transition regime, and then growing in a heat transfer controlled regime (where the evaporation rate dominates growth). A full model for both stages of growth of a bubble in both an an uniform and nonuniform superheated liquid is presented in [12].

Since we will mainly consider the case of saturated boiling in this manuscript, it is reasonable to consider the case of an uniform temperature equal to the wall temperature T_w. Additionally, owing to the properties of cryogenic liquids, the expected duration of the inertia-controlled stage of growth is very short. Hence, it is sufficient to only model the heat transfer dominated stage of growth. The radius of a growing bubble is then:

$$R_B(t) = \sqrt{\frac{12}{\pi}} \text{Ja} \sqrt{\alpha_l t} = \sqrt{\frac{12}{\pi}} \frac{\rho_l c_{p,l} \Delta T_{\text{sup}}}{h_{lg} \rho_g} \sqrt{\left(\frac{\kappa_l}{\rho_l c_{p,l}} \right) t} \tag{14}$$

---

[12]More complicated arguments include the temperature variation of the heated surface [3] or the collapse of a bubble after a previous nucleation [10], but we will utilize the simpler argument here to give an order-of-magnitude estimate.

We will note, that the general functional form $R_B = \beta\sqrt{t}$, with $\beta = f\,(\mathrm{Ja})\,\sqrt{\alpha_l}$, is common in modelling bubble growth even under different assumptions[13] [13][14][15][16]. These models might be worth considering if a more detailed analysis of the heat transfer characteristics of the cryo shields is to be performed. The Jakob number $\mathrm{Ja} = \frac{\rho_l c_{p,l} \Delta T_{\mathrm{sup}}}{h_{lg}\rho_g}$ is the ratio of sensible heat to latent heat in the evaporation process.

3.4 Bubble departure:

When the bubble grows sufficiently large, it can overcome the forces binding it to the surface where it's growing. Different authors [10] [17] argue that in the case cryogenic liquids on metallic surfaces the low contact angles ($< 15^o$ as per [11]) make it so that bubbles separate due to breaking with the edge of the nucleation sites where they grow. Following [10] and [18], the analysis for bubble detachment is carried by considering the equilibrium between buoyancy, surface tension, drag and inertial forces. In the case where we can ignore the dynamic forces, the bubble departure radius can be estimated by a balance between buoyancy and surface tension only [19]:

$$R_d = \sqrt[3]{\frac{3}{2}\frac{\sigma R_C}{g(\rho_l - \rho_g)}} \tag{15}$$

The total growth time for a bubble will then be simply given by substituting equation (15) into the bubble growth equation (14). We will then assume that the representative bubble volume V_0 from equation (10) is equal to the bubble departure volume $V_d = \frac{4\pi}{3}R_d^3$.

3.5 Nucleation rate at a single site:

Following the departure of a bubble from an active nucleation site, the cycle restarts with the reestablishment of the boundary layer. Consequently, for a single nucleation site, we expect the nucleation frequency to be:

$$f_{\mathrm{nuc}} = \frac{1}{t_d + t_w}. \tag{16}$$

Experimental observations [8][20] show that in reality there is a degree of variability on the time between successive nucleating bubbles, mostly owing to fluctuations on the waiting time t_w. We will come back to this point when we refine the model for the Newtonian Noise.

---

[13]A common, important assumption is that a microlayer of liquid forms between the growing bubble and the heated surface. This mechanism for bubble growth is frequently referenced in the modern literature, but not commonly used in analysis of cryogenic liquids, at least to the author's knowledge.

3.6 Active nucleation site density:

Estimating the number of active nucleation sites is a very challenging task, highly dependent on surface finish and on the interaction between the liquid and the heated surface. On top of that, since nucleation happens in cavities with some amount of preexisting gas, it is possible to enhance or suppress nucleation for the same surface depending on what happens before the inception of boiling.

The number of active nucleation sites is generally estimated by empirical correlations. In this case we will use the correlation by Zhokhov [21] as found in [22][14] for the number of nucleation sites per unit area as a function of the minimal radius R^*:

$$n = C_n \left(\frac{2}{R^*}\right)^m = C_n \left(\frac{\Delta T_{\text{sup}} \rho_g h_{lg}}{\sigma T_{\text{sat}}}\right)^m \tag{17}$$

$$\text{with} \quad \begin{cases} m = 2, & C_n = 10^{-7} & \text{for} \quad P/P_{\text{cr}} < 0.04 \\ m = 3, & C_n = 625 \times 10^{-16}\text{m} & \text{for} \quad P/P_{\text{cr}} \geq 0.04. \end{cases}$$

With P_{cr} being the critical pressure of the fluid, about 33.5 atm for nitrogen.

3.7 How much heat is absorbed in nucleate boiling?

It is generally agreed that during nucleate boiling there are three main components to the heat transfer: Single phase convection, evaporation and surface quenching. Summaries of this model in the case of pool boiling can be found in [24] and [23]. The heat transfer per unit area for each mechanism in the isolated bubble regime can be estimated by:

$$\text{Forced Convection:} \quad \dot{q}_{\text{fc}} = (1 - \alpha) H_{\text{fc}} (T_w - T_l) \tag{18}$$

$$\text{Evaporation:} \quad \dot{q}_{\text{evap}} = \frac{4\pi}{3} R_d^3 \rho_g n f_{\text{nuc}} h_{lg} \tag{19}$$

$$\text{Surface Quenching:} \quad \dot{q}_{\text{sq}} = \alpha \frac{2}{\sqrt{\pi}} f_{\text{nuc}} \sqrt{t_w k_l \rho_l c_{p,l}} (T_w - T_l) \tag{20}$$

Where α is the fraction of area influenced by bubble growth and it is generally estimated as $\alpha = Kn(\pi R_d^2)$ with $2 \leq K \leq 5$ [25]. The surface quenching term is related with reestablishing the boundary layer for nucleation, as discussed in Figure 2.

The three terms' relative contribution to the heat absorbed depends on the number of active nucleation sites, liquid subcooling and wall superheat. The fraction of heat absorbed by evaporation can go as low as a few percent in the isolated bubble regime [3][25] or be the dominant source for heat transfer close to the critical heat flux[15] [17].

---

[14]We use this correlation because of both its simplicity and the fact it was used successfully in [23] to predict experimental data on subcooled liquid nitrogen boiling. Since it was developed for the case of pool boiling, we expect the accuracy of the prediction to drop as we properly consider the boundary layer thickness δ in the case of flow boiling.

[15]The critical heat flux is the maximum amount of heat that can be absorbed by nucleate

3.8 Discussion and notes about the models.

The preceding section has focused in showing the main elements that go into modelling the nucleation cycle. The purpose is mainly to illustrate the important concepts and details, and we will use them to give an order-of-magnitude estimate for the Newtonian Noise. However, since the experimental conditions for boiling are very complicated, the *mechanstic* models thus presented sometimes have inaccuracies predicting the exact values for the bubble radius, nucleation frequency and number of nucleation sites that are observed in practice.

It is often the case in the literature of boiling heat transfer that researchers utilize or develop empirical correlations to estimate these parameters for their specific experimental conditions. A good account of correlations and models can be found in [26] and [27], the reader is encouraged to get acquainted with the different models[16]. Nonetheless, for our purposes the simple mechanistic models will provide sufficient knowledge for an order-of-magnitude estimate of the Newtonian noise.

3.9 First Newtonian Noise estimate:

Our first estimate for the Newtonian Noise starts by considering the a representative size of the bubbles that can nucleate at a given wall superheat

$$R_{\text{C}} \approx 3R^* = \frac{6\sigma T_{\text{sat}}}{\Delta T_{\text{sup}}\rho_g h_{lg}}. \tag{21}$$

Obtained as the active cavity size at the ONB by setting the radical of equation (12) to zero[17].

For the time being, let's consider the case of saturated boiling $T_l = T_{\text{sat}}$. In this event, the waiting time after nucleation is given by:

$$t_w = \frac{9}{4\pi\alpha_l}\left(\frac{R_C}{1-\frac{R^*}{R_C}}\right)^2 = \frac{81}{16\pi\alpha_l}\left(3R^*\right)^2 \tag{22}$$

The growth time is given by combining equations (14) and (15) as:

$$t_d = \left(\frac{R_d}{\beta}\right)^2 = \frac{\pi}{12\alpha_l}\left(\frac{9}{2}\frac{\sigma}{(\rho_l-\rho_g)}\right)^{\frac{2}{3}}\left(\frac{h_{lg}\rho_g}{\rho_l c_{p,l}\Delta T_{\text{sup}}}\right)^2\left(R^*\right)^{\frac{2}{3}} \tag{23}$$

The number of nucleation sites will follow the high pressure case for equation (17), since we assume that the liquid will need to be pressurized slightly above

---

boiling without inducing a transition to film boiling. Film boiling is a highly inefficient heat transfer mechanism and thus a safety hazard for high power cooling applications.

[16]Caution is advised, the authors have found errors in the quoted equations in the review papers, we recommend reviewing the original articles whenever possible.

[17]This is similar to the approach used in [22]. We consider it a more reasonable approach than using $R_{\text{C,max}}$ from equation (12) since it does not consider cavity flooding for high wetting liquids (such as LN2).

1 atm in order to flow. Consequently, the expected number of nucleation sites is given by:

$$N = \left(5 \times 10^{-13} \text{ m}\right) (R^*)^{-3} A. \tag{24}$$

Where A is the area of the heated surface. Naturally, given our analysis, the nucleation rate is simply: $\frac{dN}{dt} = \frac{N}{t_d + t_w}$.

Finally, it can be noted that the set of equations (21-24) are all dependent on the superheat of the cryogenic shield ΔT_{sup}. In a real system, the operating superheat will be a function of the heat load and the geometry of the array. We will give an order of magnitude assessment by considering values of ΔT_{sup} such that the fraction of the power absorbed by evaporation $\dot{Q}_{\text{evap}}$ is less than the heat load of the cooling array. A (very) conservative estimate for the heat load is around 200 W, given the design considerations of [28].

The results of the calculations are shown in Figure 4 for a couple of different (yet reasonable) values for the wall superheat. The approximate values for the physical parameters of nitrogen were taken from [29]. They are summarized in Table 1 together with the estimated values for the geometric factors of the cryo shield.

Symbol	Description	Approximate Value
ρ_l	Liquid density	830 kg/m^3
ρ_g	Gas phase density	3 kg/m^3
σ	Surface tension	10^{-2} N/m
$c_{p,l}$	Liquid specific heat	2100 J/kgK
T_{sat}	Saturation temperature	77 K
h_{lg}	Latent heat of evaporation	$2 \times 10^5 \text{ J/kgK}$
k_l	Liquid thermal conductivity	0.15 W/mK
α_l	Liquid thermal diffusivity	$8.9 \times 10^{-8} \text{ m}^2/\text{s}$
T_l	Liquid bulk temperature	77 K
D	Pipe diameter	0.01 m
L	Individual pipe length	1 m
N_{pipes}	Number of cryo pipes	4
d_0	Distance to test mass	0.5 m
C_x	Geometric factor	1

Table 1: (Top) Estimated values for physical parameters of Nitrogen, taken from [29]. (Bottom) Estimated values for the geometric and engineering parameters of the cryo array. Note that for our estimate we consider the case of saturated boiling. The geometric variables are defined in Figure 3.
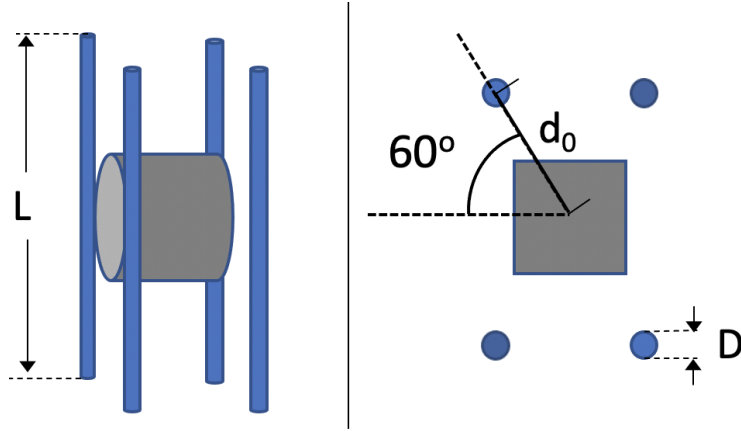
Figure 3: *Geometry of the cryo system for the Newtonian noise calculations. The values for each parameter are summarized in Table 1. For simplicity, we consider 4 tubes 60 degrees of the longitudinal direction from the test mass. We also simplify the masses of each tube to lie in the vertical midpoint of the array. Since the noise for every tube is considered to be independent, the geometric factor of this array is $C_x = 4\cos^2(60^o) = 1$.*

Symbol	Description	Calculated Values	Units
ΔT_{sup}	Wall superheat	0.5 , 1.5 , 2.0	K
R_C	Representative cavity radius	12 , 4.1 , 3.1	µm
R_d	Bubble departure radius	0.27 , 0.19 , 0.17	mm
t_d	Bubble growth time	140 , 7.5 , 3.5	ms
t_w	Waiting time	2.7 , 0.30 , 0.17	ms
f_{nuc}	Nucleation frequency	7 , 130 , 270	Hz
n	Active nucleation site density	0.74 , 20 , 47	sites/cm^2
$\dot{Q}_{\text{evap}}$	Power absorbed by evaporation	0.38 , 63 , 240	W

Table 2: Calculated values for the nucleation parameters based on equations (17-23) and the values of Table 1. We evaluate three conditions for the wall superheat (0.5, 1.5 and 2.0 K) to cover the likely operating range for the cryo shield. The values for $\dot{Q}_{\text{evap}}$ consider the geometry shown in Figure 3.
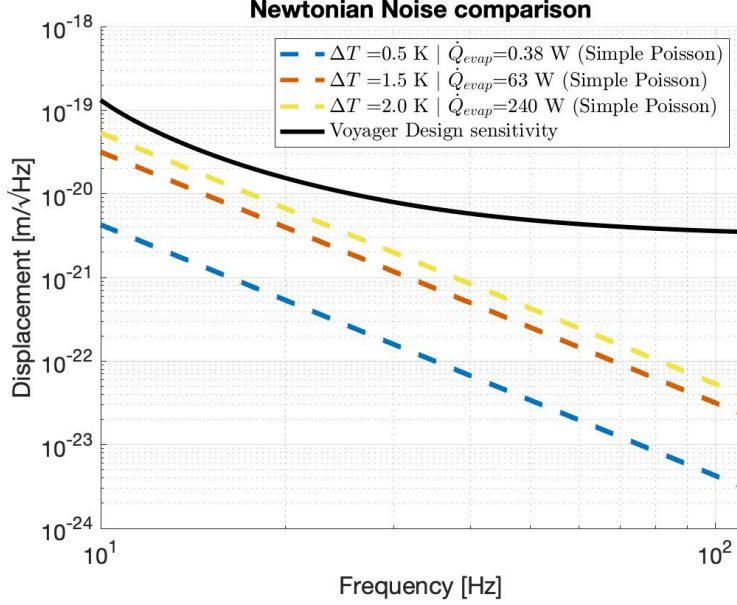
Figure 4: *First estimate for the Newtonian noise coupling using the Poisson model (10). For reference, The nucleation frequencies f_{nuc} estimated for $\Delta T_{sup} = 0.5$, 1.5 and 2 K; were 7, 130 and 270 Hz respectively. All of the values for important parameters for the estimates are summarized Tables 1 and 2.*

3.9.1   Discussion:

There are a few conclusions we can immediately draw by looking at the simple estimate from Figure 4:

- The expected noise amplitude falls as $1/f^3$. In reality this dependence will roll off due to the finite growth and travel time of the bubbles.

- The noise amplitude increases as the heat absorbed by evaporation $\dot{Q}_{\text{evap}}$ increases. The reason for this increase can be traced in our model to the drastic increase of the nucleation rate for high wall superheats:

- We note that for nitrogen, in the range of parameters we are considering, $t_d/t_w < 10$ and it is a reasonable estimate to make $f_{\text{nuc}} = 1/t_d$. In that case

$$V_0\sqrt{\frac{dN}{dt}} \propto \beta\left(R^*\right)^{-\frac{5}{6}} \quad \text{and} \quad V_0\frac{dN}{dt} \propto \beta^2\left(R^*\right)^{-\frac{8}{3}} \tag{25}$$

We know that β is an increasing function of the wall superheat[18] and the critical radius R^* decreases with it. The end result is that when the wall

---

[18]This is true under other assumptions about bubble growth too.

14

superheat increases, both the power absorbed and the Newtonian noise will increase.

In consequence, if we want to mitigate the Newtonian noise coupling by a factor of 10, we would have to sacrifice on a factor of more than 100 of the heat transfer gains from the evaporation component of boiling.

- The estimated noise amplitude is below the design sensitivity for LIGO Voyager [28] for $\dot{Q}_{\text{evap}} < 200$ W. This is the (conservative) estimate for the heat load on the outer shield of the cryo array.

Apart from these conclusions, our dive into the theory of boiling and nucleation exposed a couple oversights in the original argument for modelling the Newtonian Noise coupling. The most important of them has to do with the inherent periodicity of the nucleation process. Followed closely by the fact that neighboring nucleation sites exert influence on one another [16].

The first of these two points will cause peaks in the displacement spectrum at f_{nuc} and its harmonics, and could potentially be a dealbreaker in terms of using boiling as the main heat transfer mechanism during operation of the interferometer. While the second one can potentially increase the overall baseline of the coupling estimated in Figure 4 by coherently adding the influence of neighboring nucleation sites.

We will qualitatively address the influence of these two phenomena by borrowing from the literature on quasiperiodic point processes in the next section. Concluding with a quantitative estimate that addresses the first point about the appearance of spectral peaks.

4 Renewal Shot Noise

This section introduces the concepts needed to make a refined estimate for the spectra shown in Figure 4. The main ingredient we will use are results from renewal theory and the spectrum of renewal point processes. Renewal shot noise allows us to analyze the spectrum of the Newtonian noise if the release times between two successive bubbles are not independent.

In what follows we will show the most important results in an informal language suited for the discussion on Section 5. The precise mathematical formulations of equations can be found in [4], also summarized in [5][19]. For more general renewal theory information regarding renewal theory [30] is a good reference.

4.1 Theoretical overview:

A *point process* is a discrete (but infinite) collection of events in a mathematical space. For our purposes, they will represent the set of times $\{t_i\}$ in which a given nucleation site starts the nucleation cycle anew.

---

[19]Renewal shot noise is of interest to the neuroscience community, where it is used to model the spectra of firing neurons.

The (possibly time-dependent) *rate* $r(t)$ of the process is the average number of occurrences $\{t_i\}$ in a short time interval around a time t of interest.

Consider the $\delta-$spike train associated with the point process:

$$\phi(t) = \sum_i \delta(t - t_i) \tag{26}$$

Then the rate is just an ensemble average over different realizations of the point process: $r(t) = < \phi >_{\text{ens}}$. If the process is stationary and ergodic, the rate is constant and we can change the ensemble average by a time average. For our estimates, the rate of the point process is simply the nucleation frequency at a single nucleation site, thus $r = f_{\text{nuc}}$.

Additionally, given a function $h(t)$ (like the one in equation (6)) that represents a physical response that repeats itself at intervals $\{t_i\}$ from a point process, the function $H(t)$ formed by the superposition of those responses is a convolution of h with the $\delta-$train of the process:

$$H(t) = \sum_i h(t - t_i) = (h * \phi)(t) \tag{27}$$

The average (or DC value) of H is given by Campbell's theorem [6]:

$$< H >= r \int_{-\infty}^{\infty} h(\tau) \ d\tau, \tag{28}$$

And the amplitude spectrum of fluctuations around the mean is:

$$|\delta\hat{H}(f)| = |\hat{h}(f)||\delta\hat{\phi}(f)|. \tag{29}$$

This last equation can be seen as the Fourier transform of equation (27), where we subtracted the DC value of the signal.

In consequence, the determination of the spectrum of H hinges on determining the spectrum for the $\delta-$train associated with the point process.

4.1.1 The spectrum of the $\delta-$train:

Following the Wiener-Khinchin Theorem, the power spectrum of ϕ can be related to the autocorrelation function of the $\delta-$train. Since we are considering a stationary process, in order to compute the autocorrelation it is sufficient to know the conditional probability that there will be another event at a time $t = \tau$ given that there was one at time $t = 0$.

This analysis eventually leads to the following expression for the (single sided) power spectrum of the fluctuations of ϕ [4][5]:

$$|\delta\hat{\phi}(f)|^2 = 2r \left(1 + 2\text{Re} \left(\sum_{n=1}^{\infty} \hat{\rho}_n(f) \right) \right) \tag{30}$$

Where $\rho_n(\tau)$ is the probability density of the $n-$th order time interval. Or the conditional probability that the $n-$th bubble after will come out at time $t = \tau$, given that a bubble came out at time $t = 0$.

16

From equation (30) it is evident that the defining variables of the spectrum are the probability distributions between different nucleated bubbles. Therefore, by choosing an appropriate set of ρ_n, it is possible to refine the estimate from Figure 4.

4.1.2   Spectrum of a renewal process:

For simplicity, we will model the nucleation cycle as a *Renewal process*, that is as a set of independent and identically distributed *interarrival times* $\tau_i = t_{i+1} - t_i$ between successive nucleating bubbles, all drawn from the same probability distribution $\rho_1(\tau)$.

The intuition behind this choice is that the set $\{\tau_i\}$ represents the waiting and growth times of a each bubble generated in a nucleation site. We consider each bubble to be generated independently, which is a more accurate picture for nucleation than the Poisson shot noise presented before[20]. The distribution $\rho_1(\tau)$ can be found from experimental observations [8][20].

Since different bubbles are independent, we have $\hat{\rho}_n(f) = (\hat{\rho}_1(f))^n$. Substitution in (30) and a geometric series yield the spectrum of the $\delta-$train at a single site:

$$|\delta\hat{\phi}(f)|^2 = 2r\left(\frac{1 - |\hat{\rho}_1(f)|^2}{|1 - \hat{\rho}_1(f)|^2}\right) \tag{31}$$

We conclude the estimate by assuming that the nucleation sites are all independent, which implies that their renewal spectra add in quadrature [31]. If we assume (conservatively) that all of them nucleate at the same rate $r = f_{\text{nuc}}$ and possess the same distribution $\rho_1(\tau)$, the amplitude spectra for the Newtonian-noise induced displacement will be given by a modified version of equation (10):

$$|\delta\hat{x}(f)| = \sqrt{2}\frac{C_x}{(2\pi f)^3}\frac{G}{d_0^2}(\rho_l - \rho_g)V_0\sqrt{\frac{dN}{dt}}\sqrt{\frac{1 - |\hat{\rho}_1(f)|^2}{|1 - \hat{\rho}_1(f)|^2}} \tag{32}$$

As a side note, the Poisson shot noise is recovered in (32) by choosing $\rho_1(\tau)$ as the exponential distribution[21].

4.2   Qualitative remarks about renewal shot noise

Figure 5 shows a comparison of the renewal shot noise spectrum between different choices for the internucleation time distribution ρ_1. For illustrative purposes, all distributions have the same nucleation frequency $r = f_{\text{nuc}} = 100$ Hz.

The first thing that can be appreciated is that as ρ_1 becomes more centered around its mean, peaks start to emerge in the amplitude spectrum. The peaks

---

[20]In the Poisson shot noise assumption, all times $\{t_i\}$ are considered independent. Under the renewal shot noise assumption only the difference between successive times is considered independent. This change alone will allow us to account for the inherent periodicity of the nucleation process.

[21]This is related to the fact that the exponential distribution is the only *memoryless* distribution. No time interval is different from the others, implying that there is no long-range order and no special frequencies for the spectrum to peak at.

appear at multiples of f_{nuc} and become sharper as deviations around the average internucleation time decrease.

It can also be noted that all the spectra look flat at high enough frequencies. For timescales shorter than the deviations around the mean, the renewal process looks as random as the regular shot noise[22]. As a side note, choosing ρ_1 the exponential distribution recovers the Poisson shot noise (flat) spectrum.

Finally, the spectral density is always smaller at low frequencies for the Renewal processes than for the Poisson process. This observation was also made by Bartlett [4], and it is related to the decreased variance of the probability distribution ρ_1 relative to its mean. It is also mentioned in [4] that effects like clustering (or, in our case, correlations between adjacent nucleation sites) increase the low-frequency content of the spectra. These two competing effects could conceivably cancel each other out, but by no means do they imply that the spectral peaks would disappear.
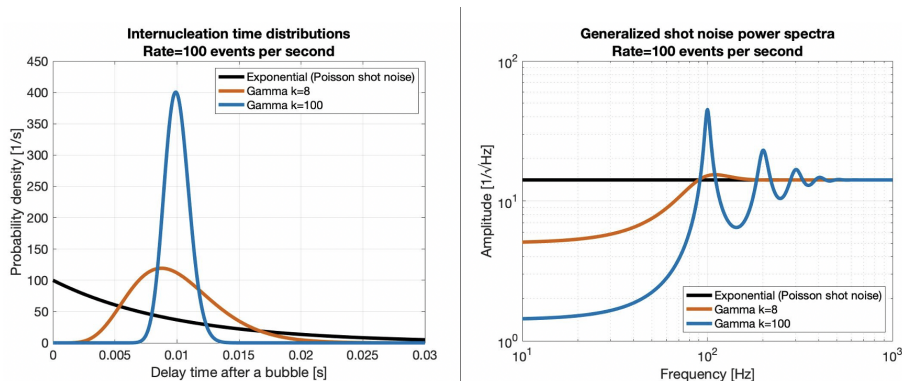

Figure 5: *Comparison between the spectra of the $\delta-$train defined in equation (26) for point processes with the same event rate but different distributions. (Left) Example distributions for the difference between successive nucleation times $\tau_i = t_{i+1} - t_i$. (Right) Generalized shot noise spectra associated with each different distribution. The exponential distribution, which represents the case of Poisson shot noise, is included for comparison.*

4.3 Newtonian noise estimate with renewal shot noise

In order to refine the estimate from Figure 4 with renewal shot noise, we need to select a distribution $\rho_1(\tau)$ that describes the observed behavior of the time interval between nucleations at the same site. Based on the results from [8] and the internucleation distribution plotted in [20], we decided to use a gamma distribution:

---

[22]An interpretation is that the high frequency components cannot capture the long-timescale order between successive nucleations.

$$\rho_1(\tau) = p_{k,\theta}(\tau) = \frac{1}{\Gamma(k)\theta^k}\tau^{k-1}e^{-\frac{\tau}{\theta}} \quad , \quad \tau \geq 0, \tag{33}$$

which has the advantage of both being flexible and easy to compute. The Fourier transform of this distribution is:

$$\hat{\rho}_1(f) = \frac{1}{(1 - 2\pi i\theta f)^k}. \tag{34}$$

For our calculations, we choose k and θ such that the average time satisfies $<\tau> = t_d + t_w$ and the standard deviation is one percent of the mean[23] ($\sqrt{<\Delta\tau^2>}/\tau = 0.01$). The results of the Newtonian noise modelling with equation (32) are shown in Figure 6. The parameters used are the same as for Figure 4, and are summarized in Tables 1 and 2.
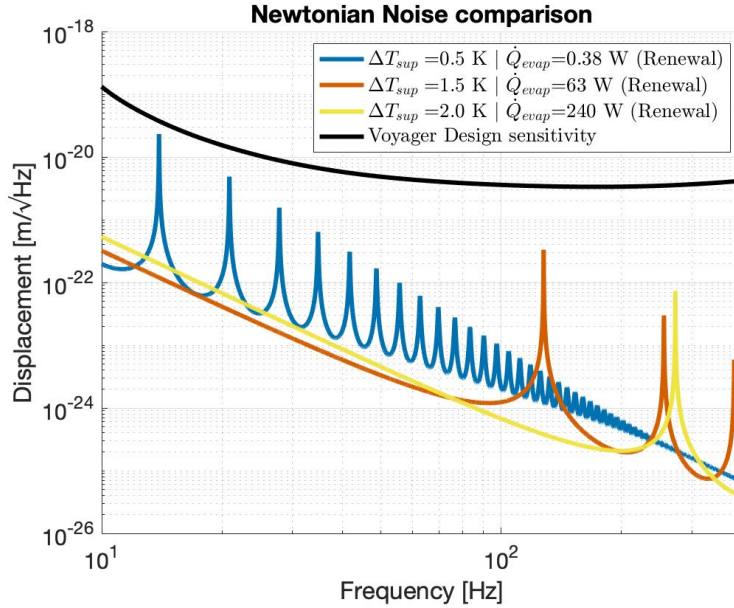

Figure 6: *Second estimate for the Newtonian noise coupling, this time including insight from renewal theory. The values for all parameters are identical to those of Figure 4. The peaks in the spectrum correspond to the multiples of the nucleation frequencies (f_{nuc}= 7, 130 and 270 Hz) for each condition.*

4.4 Discussion:

We can observe that the inclusion of the periodic effects has a big impact on the estimated Newtonian noise coupling. First, we observe there are peaks at

---

[23]This choice is based on the observation that t_w/t_d in Table 2 was in the range of a percent. It leads to $k = (0.01)^{-2}$ and $\theta = (t_d + t_w)/k$.

multiples the nucleation frequencies f_{nuc} for each different value of the wall superheat. The peaks in the spectra reach as high as an order of magnitude above their flat spectrum values. Our order-of-magnitude estimates remain below the LIGO Voyager design sensitivity from [28], but the presence of peaks would still make the Newtonian noise one of the primary contributors to the noise budget for the interferometer.

Another important observation from Figure 6 is that due to the overall $1/f^3$ dependence of the noise, it is advantageous to have a higher value of f_{nuc}. That way, if there is any peaking, it will occur where the Newtonian noise's baseline is thousands of times below design sensitivity.

As a side-note, we will also mention that these estimates represent a worst-case scenario where all of the active nucleation sites nucleate at a frequency f_{nuc}. In reality, the effects of different sites will tend to average out, smoothing the peaks and potentially leading to a lower coupling at low frequencies.

5 Summary of results and discussion:

The results shown on figures 4 and 6 and the important insights from the theory of nucleation as well as point processes are summarized below:

- The estimated levels of Newtonian noise for a cryogenic array were estimated to be below the design sensitivity of LIGO Voyager for a reasonable set of parameters and a heat load of $\dot{Q} < 200$ W. This holds true even if we consider that all nucleation sites have a characteristic nucleation frequency f_{nuc}.

- The noise spectrum falls off as $1/f^3$, with the possibility of extra suppression at higher frequencies due to the finite travel time of the bubbles.

- The inherent periodicity of the nucleation process can lead to peaks in the Newtonian noise spectrum. The peaks appear at multiples of the nucleation frequency and can rise above the noise's baseline by an order of magnitude.

- Clustering effects, like the correlation between nearby nucleation sites have the potential to increase the low frequency component of the Newtonian noise.

- The baseline for the Newtonian noise increases with increasing nucleation frequency. However, since the peaks on the noise spectrum move to a higher frequency, the $1/f^3$ suppression decreases their contribution to the noise budget.

- From equation (23) we observe that the departure frequency increases as we decrease the active cavity radius R_C. Said differently, smaller bubbles nucleate faster.

- Nucleate boiling will occur as long as cavities in the active range $\{R_{C,max}, R_{C,min}\}$ from equation (12) are available on the surface of the heated channel. Cavity flooding and surface treatment could change this.

- Attempting to decrease the Newtonian noise can result in a significant reduction of the heat transfer characteristics of the cooling array, as shown in Figure 4.

- The results shown are only valid if we can disregard the interaction between bubbles. At high enough void fractions this is no longer true. Bubble coalescence can form slugs that would have a more deleterious effect.

5.1 Recommendations for Design:

Given all of the information we have gathered, we believe it would be beneficial to suppress nucleation for the steady state operation of the interferometers. Primarily, due to the potential presence of spectral peaks, and secondarily, to avoid other unintended couplings such as acoustic noise or scattered light noise coming from the nucleation process.

In order of probable impact, here is a short list of the measures we think would aid with the suppression of nucleate boiling during steady state operation of the cryo array[24]:

- **Use subcooled nitrogen:** Nitrogen can remain liquid between approximately 63 and 77 K at a pressure of 1 atmosphere. A potential option to suppress nucleation then is to run subcooled nitrogen (say, at 65 K) and take advantage of the high specific heat to provide cooling.

  - The range of temperatures where Nitrogen remains liquid can be widened by increasing the operating pressure [29][32]. At a pressure of 2 atm, the saturation temperature increases to about 84 K, with little change on the freezing temperature or the specific heat. This could be used to further amplify the liquid's ability to absorb heat without resorting to boiling.

- **Surface treatment:** The inner walls of the tubes can be treated to reduce the number of potential nucleation sites. The main objective of this treatment is to reduce the number of cavities in the active range (12) given the likely cryo shield superheat ΔT_{sup}.

  - An alternative way to think about this is that if we can ensure there are no cavities of radius greater than a tolerance ϵ, then the wall superheat needed to initiate nucleation is $\Delta T_{sup} \geq \frac{2\sigma T_{sat}}{\epsilon \rho_g h_{lg}}$. For example, if $\epsilon = 0.1$ µm, we need $T_{sup} \geq 20$ K to initiate nucleation.

---

[24]This is not an exhaustive list, and many of the options proposed can be used simultaneously to achieve good operating conditions for the cryo array.

- **Faster liquid Flow:** An implicit assumption for the equations derived in the theory of nucleation is that the thermal boundary layer δ is thick enough to sustain nucleation. It is possible, to suppress nucleation without surface treatment by flowing subcooled liquid at a high enough velocity: through an increase in H_{fc}[25], we can reduce the thickness of the thermal boundary layer, increasing the necessary wall superheat for the ONB.

- **Surface Treatment + Artificial nucleation sites:** In the event where we would like to suppress nucleation but not completely give up on the enhanced heat transfer characteristics of boiling, we can complement the surface treatment approach with etching artificial nucleation sites. The main points to consider are to keep the nucleation site density n low enough to maintain the overall Newtonian noise level low and to use small enough crevices such that their nucleation frequency f_{nuc} is unlikely to have a big impact on the interferometer's noise budget (similar to the 2 K example from Figure 6).

References

[1] B. Shapiro, R. X. Adhikari, O. Aguiar, E. Bonilla, D. Fan, L. Gan, I. Gomez, S. Khandelwal, B. Lantz, T. MacDonald, *et al.*, "Cryogenically cooled ultra low vibration silicon mirrors for gravitational wave observatories," *Cryogenics*, vol. 81, pp. 83–92, 2017.

[2] S. M. Ghiaasiaan, *Two-phase flow, boiling, and condensation: in conventional and miniature systems.* Cambridge University Press, 2007.

[3] L. S. Tong, *Boiling heat transfer and two-phase flow.* Routledge, 2018.

[4] M. S. Bartlett, "The spectral analysis of point processes," *Journal of the Royal Statistical Society: Series B (Methodological)*, vol. 25, no. 2, pp. 264–281, 1963.

[5] B. Lindner, "A brief introduction to some simple stochastic processes," *Stochastic Methods in Neuroscience*, vol. 1, 2009.

[6] W. Van Etten, *Introduction to random signals and noise.* Wiley Online Library, 2005.

[7] Y. Hsu, "On the size range of active nucleation cavities on a heating surface," 1962.

[8] H. Chi-Yeh and P. Griffith, "The mechanism of heat transfer in nucleate pool boiling—part ii: the heat flux-temperature difference relation," *International Journal of Heat and Mass Transfer*, vol. 8, no. 6, pp. 905–914, 1965.

---

[25]Flow with higher Reynolds numbers have better forced convection heat transfer. See, for example, the Dittus-Boelter correlation in [2].

[9] S. Kandlikar, "Heat transfer characteristics in partial boiling, fully developed boiling, and significant void flow regions of subcooled flow boiling," 1998.

[10] W. Bald, "Cryogenic heat transfer research at oxford: Part 1—nucleate pool boiling," *Cryogenics*, vol. 13, no. 8, pp. 457–469, 1973.

[11] P. Brennan and E. Skrabek, "Design and development of a prototype static cryogenic heat transfer system,'," *NASA CR-121939*, 1971.

[12] B. Mikic, W. Rohsenow, and P. Griffith, "On bubble growth rates," *International Journal of Heat and Mass Transfer*, vol. 13, no. 4, pp. 657–666, 1970.

[13] D. Labuntsov, "Study of the growth of bubbles during boiling of saturated water within a wide range of pressures by means of high-speed moving pictures," *Teplofizika Vysokikh Temperatur*, vol. 2, no. 3, pp. 446–453, 1964.

[14] M. Cooper, "The microlayer and bubble growth in nucleate pool boiling," *International Journal of Heat and Mass Transfer*, vol. 12, no. 8, pp. 915–933, 1969.

[15] R. Cole and H. L. Shulman, "Bubble growth rates at high jakob numbers," *International Journal of Heat and Mass Transfer*, vol. 9, no. 12, pp. 1377–1390, 1966.

[16] N. I. Kolev and N. Kolev, *Multiphase flow dynamics*, vol. 1. Springer, 2005.

[17] Y. A. Kirichenko, L. Slobozhanin, and N. Shcherbakova, "Analysis of quasi-static conditions of boiling onset and bubble departure," *Cryogenics*, vol. 23, no. 2, pp. 110–112, 1983.

[18] Y. A. Kirichenko, V. Tsybul'Skii, M. Dolgoi, K. Rusanov, and I. Konovalov, "Effect of pressure on internal characteristics of nitrogen and oxygen boiling," *Journal of engineering physics*, vol. 28, no. 4, pp. 409–414, 1975.

[19] Y. A. Kirichenko, "Evaluation of the conditions of vapor bubble separation during nucleate boiling," *Journal of engineering physics*, vol. 25, no. 1, pp. 811–817, 1973.

[20] D. Euh, B. Ozar, T. Hibiki, M. Ishii, and C.-H. Song, "Characteristics of bubble departure frequency in a low-pressure subcooled boiling flow," *Journal of nuclear science and technology*, vol. 47, no. 7, pp. 608–617, 2010.

[21] K. Zhokhov, "Number of vapor-forming centers," *Trudy TsKTI*, no. 91, 1968.

[22] Y. A. Kirichenko, M. Dolgoj, N. Levchenko, V. Tsybul'skij, L. Slobozhanin, and N. Shcherbakova, "Study on cryogenic liquid boiling," 1976.

[23] X. Li, W. Wei, R. Wang, and Y. Shi, "Numerical and experimental investigation of heat transfer on heating surface during subcooled boiling flow of liquid nitrogen," *International Journal of Heat and Mass Transfer*, vol. 52, no. 5-6, pp. 1510–1516, 2009.

[24] R. Judd and K. Hwang, "A comprehensive model for nucleate pool boiling heat transfer including microlayer evaporation," 1976.

[25] D. Kenning *et al.*, "Fully-developed nucleate boiling: overlap of areas of influence and interference between bubble sites," *International Journal of Heat and Mass Transfer*, vol. 24, no. 6, pp. 1025–1032, 1981.

[26] V. Guichet, S. Almahmoud, and H. Jouhara, "Nucleate pool boiling heat transfer in wickless heat pipes (two-phase closed thermosyphons): A critical review of correlations," *Thermal Science and Engineering Progress*, vol. 13, p. 100384, 2019.

[27] G. H. Yeoh and X. Zhang, "Computational fluid dynamics and population balance modelling of nucleate boiling of cryogenic liquids: Theoretical developments," *The Journal of Computational Multiphase Flows*, vol. 8, no. 4, pp. 178–200, 2016.

[28] R. X. Adhikari, O. Aguiar, K. Arai, B. Barr, R. Bassiri, G. Billingsley, R. Birney, D. Blair, J. Briggs, A. F. Brooks, *et al.*, "A cryogenic silicon interferometer for gravitational-wave detection," *arXiv preprint arXiv:2001.11173*, 2020.

[29] J. Jensen, R. G. Stewart, W. Tuttle, and H. Brechna, *Brookhaven national laboratory selected cryogenic data notebook: sections I-IX*, vol. 1. Brookhaven National Laboratory, 1980.

[30] D. R. Cox, "Renewal theory," 1962.

[31] B. Lindner, "Superposition of many independent spike trains is generally not a poisson process," *Physical Review E*, vol. 73, no. 2, p. 022901, 2006.

[32] R. T. Jacobsen, R. B. Stewart, and M. Jahangiri, "Thermodynamic properties of nitrogen from the freezing line to 2000 k at pressures to 1000 mpa," *Journal of Physical and Chemical Reference Data*, vol. 15, no. 2, pp. 735–909, 1986.